IMPROVED INGAAS METAL-SEMICONDUCTOR-METAL OE MIXERS USING SUBMICRON SCHOTTKY CONTACTS

Rishabh Mehandru[a], Keith Aliberti[b], Hongen Shen[b], *Soohwan Jang[a], S. J. Pearton[c], and Fan Ren[a]

a Department of Chemical Engineering, University of Florida, Gainesville, FL 32611

b U. S. Army Research Laboratory, 2800 Powder Mill Road Adelphi, MD 20783

c Department of Materials Science and Engineering, University of Florida, Gainesville, FL 32611

Abstract

InGaAs-based Metal Semiconductor Metal (MSM) Photodetectors were fabricated and tested as photodetectors and Opto-electronic mixers. A comparison of various processing schemes for MSM InAlAs/InGaAs photodetectors on InP substrates was conducted to minimize the dark current. InAlAs Schottky Enhanced Layers (SEL) was employed on the InGaAs-based MSMs to enhance the barrier height to reduce the dark current. The effect of SEL thickness on the performance of OE mixer was studied. The experimental results were compared to those simulated with CFDRC software.

Introduction

LADAR Systems utilize laser light for the detection of object speed, altitude, direction and range. Military interest in LADAR has been ongoing for a number of years, particularly for target identification and range determination. [1.2] In general, there are two types of ranging techniques used in LADAR to measure the time delay from the sensor to the target. One technique measures the time delay using short pulses of laser light: this technique requires the use of high-bandwidth receivers. The other technique measures the time delay using modulation waveforms impressed on continuous-wave (cw) lasers: this technique requires suitable-bandwidth receivers. Both techniques can be implemented using direct detection or optically coherent receivers.[3,6]

The U.S. Army Research Laboratory (ARL) is developing low-cost LADAR Systems that utilize diode-laser transmitters. Diode lasers cost significantly less than solid state lasers and are more electrically efficient. Pulsed diode lasers suffer from limited peak power capability due to damage at the output laser facet that, in a typical pulse operation, limit the amount of total energy that can be focused onto a target. Low-cost cw laser diodes, however, with optical power levels in the low Watts, are available commercially. With this in mind, ARL began investigating a unique, optically incoherent, LADAR architecture that uses frequency-modulated, continuous-wave (FM/cw) radar principles. [7-10] In this architecture, transmit and receive radar antennas are replaced by an intensity-modulated cw semiconductor laser diode and an optical receiver, respectively.

LADAR operation in the infrared, mainly 1.55 μm, would help render the system eye-safe. For this application, InGaAs-based MSM-PD OEMs are necessary. Unfortunately, the Schottky barrier height on InGaAs is quite low (~0.1-0.2 eV) leading to high dark current and, hence, low signal-to-noise ratio. To reduce dark current, the Schottky barrier height must be "enhanced". Typically, this is accomplished by growing

Report Documentation Page

Form Approved
OMB No. 0704-0188

1. REPORT DATE	2. REPORT TYPE	3. DATES COVERED
00 DEC 2004	**N/A**	**-**

4. TITLE AND SUBTITLE	5a. CONTRACT NUMBER
Improved Ingaas Metal-Semiconductor-Metal Oe Mixers Using Submicron Schottky Contacts	5b. GRANT NUMBER
	5c. PROGRAM ELEMENT NUMBER
6. AUTHOR(S)	5d. PROJECT NUMBER
	5e. TASK NUMBER
	5f. WORK UNIT NUMBER
7. PERFORMING ORGANIZATION NAME(S) AND ADDRESS(ES) **Department of Chemical Engineering, University of Florida, Gainesville, FL 32611; U. S. Army Research Laboratory, 2800 Powder Mill Road Adelphi, MD 20783**	8. PERFORMING ORGANIZATION REPORT NUMBER
9. SPONSORING/MONITORING AGENCY NAME(S) AND ADDRESS(ES)	10. SPONSOR/MONITOR'S ACRONYM(S)
	11. SPONSOR/MONITOR'S REPORT NUMBER(S)

12. DISTRIBUTION/AVAILABILITY STATEMENT
Approved for public release, distribution unlimited

13. SUPPLEMENTARY NOTES
See also ADM001736, Proceedings for the Army Science Conference (24th) Held on 29 November - 2 December 2005 in Orlando, Florida. , The original document contains color images.

14. ABSTRACT

15. SUBJECT TERMS

16. SECURITY CLASSIFICATION OF:			17. LIMITATION OF ABSTRACT	18. NUMBER OF PAGES	19a. NAME OF RESPONSIBLE PERSON
a. REPORT	b. ABSTRACT	c. THIS PAGE			
unclassified	**unclassified**	**unclassified**	**UU**	**8**	

(e.g. via molecular beam epitaxy) high-band-gap, lattice-matched InP or InAlAs Schottky enhancement layers (SELs) on top of the InGaAs layer. Photodetectors using Schottky enhancement layers (SELs) have been shown to yield low dark current, high responsivity, and high bandwidth. [8-16]

In this talk, various device designs and processing schemes of InGaAs based 1.55 μm inter-digitated metal-semiconductor-metal (MSM) photo-detectors will be presented. A simple circuit model was employed to explain the mixing results. Another more comprehensive semiconductor device model coupled with electromagnetic optics was used to simulate the dc and pulse responses of the MSM devices and good agreements with the experimental results were obtained. The simulations helped understand the nature of so called "knee" in the photo dc IV characteristics of the MSM photodetector. As a result of simulation, a thinner SEL structure was utilized and the mixing characteristics were greatly improved.

Experimental

Our metal-semiconductor-metal (MSM) structure consists of a 500 or 100Å InAlAs/InGaAs Schottky barrier enhancement layer, a 150-Å In(Ga,Al)As graded layer, a 1.0-μm InGaAs active layer, and a 0.3-μm InAlAs buffer layer grown on a semi-insulating InP:Fe substrate with a molecular-beam epitaxy (MBE) system. All levels of the devices were made using standard optical lithography except some of the MSM fingers were defined with a Raith electron beam direct write system. Electron-beam deposited Ti/Au metallization was used for Schottky and final metal contacts. Plasma enhanced chemical vapor deposited SiN_x and SiO_2 were employed for device passivation. CF_4/O_2 based plasma and $H_2SO_4/H_2O_2/H_2O$ based wet-chemical etchant were used for dielectric etching and mesa definition.

Room temperature dark current measurements were performed using an HP4145B parameter analyzer. High speed measurements were conducted with a mode-locked Ti-sapphire laser-pumped optical parametric oscillator delivering 1.3-1.55-μm optical pulses at 76-MHz and power was tunable to 3-nJ. The pulses passed through a continuously variable inline attenuator for power control and a beam splitter for power monitoring and the pulses were focused onto the device using a lens and a precision-adjustment stage. The high-speed signal was measured via two DC-to-40-GHz ground-signal-ground microwave probes attached through short transmission lines to a 40-GHz-digitizing oscilloscope.

Mixing characteristics were measured with light from an amplitude-modulated 1.55-μm, 10-Gb/s, fiber-pigtailed laser. Optical power was adjusted via a continuously-variable, in-line, fiber-coupled attenuator. The LO bias was applied to one electrode, shunted with a 50-ohm termination, and the mixed signal was recovered from the other electrode, which was connected to a spectrum analyzer through a low-pass filter.

Results and Discussion

(1) Different Processing Sequences

To achieve very low dark current, high speed and high responsive goal, three different processing schemes were employed. In all of the processing schemes, the final metal contact pads were deposited on the top of a dielectric layer to reduce leakage current and capacitance resulting from the relatively large area of the final metal contact pads as compared to the actual device area. High leakage current means high dark current (high noise) and high capacitance means slower RC response in high frequency applications.

In the first MSM process scheme, Ti/Au (200Å/1800Å) based Schottky MSM fingers and finger-

connections were deposited on top of the InGaAs/InAlAs MQW, followed by 1000 Å of Si_3N_4 and then 1850Å of SiO_2. The thickness of dielectric films was determined through a simulation so as to have reflection losses of less than 5% in the wavelength of interest. Then a contact window was opened in the dielectric layer to contact the metal finger-connections. The Ti/Au (200Å/2500Å) based final metal contact pads connected the MSM Schottky fingers through the dielectric window. In this process scheme, the dark current was generated from the MSM Schottky fingers as well as metal finger-connections. The second scheme employed a dielectric window. The metal finger-connections and finger-tips sit on the top of dielectric film. Contact widows were opened the mesa window in the dielectric film (which was 2600 Å of Si_3N_4) by dry etch and wet etch in succession. The final few 100 Å of dielectric was removed by wet etch to avoid any plasma damage.

Dark current measurements were performed to determine the efficiency of each design in reducing noise. The measurements showed that the second processing scheme was more efficient in reducing the dark current. Dark current of less than 0.1 nA at a bias of 1V was obtained, as shown in the current-voltage (I-V) characteristics of Figure 1. The dark current with the first processing scheme was on the order of 60 nA for a device of length 30 μm, finger width 1 μm and finger spacing 3 μm. In the second processing sequence, since the contact finger-tips were laying on top of the dielectric film, the dark current was greatly reduced. The electric field was also much more concentrated on the tip resulting in large leakage in the first case. This was further proven for measurements on a few devices in which their Schottky level was misaligned. The tips for these devices were on the semiconductor surface instead of the dielectric surface. These photodetectors displayed dark currents on the order of few 10's of nano Amps. There was also an increase in the dark current with increase in device size as shown in Figure 1.

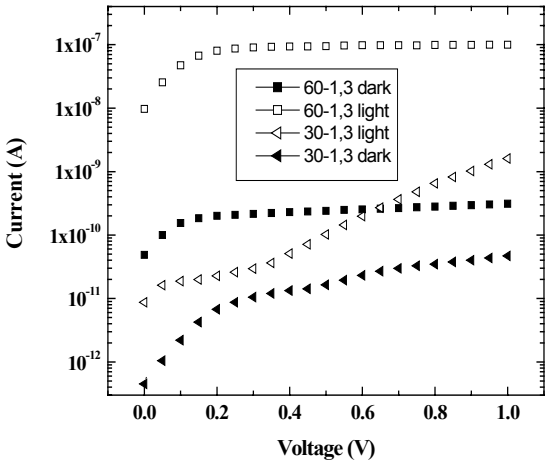

Fig. 1: Measured I-V response of the device processed with the second type of fabrication sequence. The devices had lengths of 60 μm or 30 μm and finger widths of 1μm and finger spacing of 3 μm.

To further enhance the temporal response of the MSM detector without losing the advantage of low dark current, an etch-back process was developed. The mesa was etched first, and then a dielectric equal in height to this mesa was deposited using PECVD. Planarization of the dielectric film was achieved with a polymer coating and a planarization coating etch-back to expose dielectric top. Then, the etch chemistry was switched to etch the dielectric using the planarization coating as a mask to expose the top surface of the semiconductor. The planarization coating was subsequently removed with acetone at the completion of the process. The dark current was less than 1nA at 1V and the device was highly linear in response to the different levels of microscope light. The dark current is slightly higher than for the second fabrication sequence, which may be resulting from the plasma etch damage during the etch - back process. The damage can be reduced by switching the dry etch to wet chemical etching for the last few hundred angstroms of the dielectric film.

Sub-micron finger width MSM-PDs were also fabricated using electron beam lithography. MSM-PDs with finger widths as low as 0.1 µm were achieved. Figure 2 shows SEMs of submicron Schottky metal fingers. The metal step over the dielectric is smooth as shown in the high resolution (100 KX) SEM image. The comparison of dark current with different finger width on 100 Å InAlAs SEL sample is shown in Figure 2 (a). The dark current is reduced by an order of magnitude by writing sub-micron fingers. Figure 2 (b) compares fingers with different submicron area but with same periphery. It can be seen that the dark current is strongly dependent on finger area, indicating that the current flows uniformly underneath the metal finger. Reduced finger width increases signal to noise ratio, hence improving bandwidth of the OE Mixer.

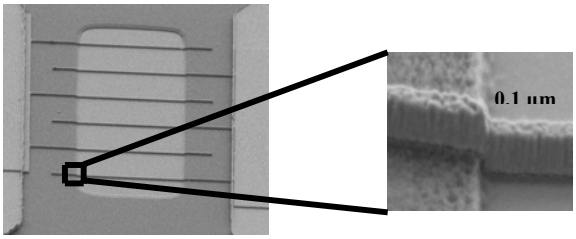

Fig. 2: SEM image of submicron finger width MSM detector with finger width of 0.2 µm.

(2) 2–Dimensional simulation of pulse response, DC light response and mixing characteristics of Schottky-barrier-enhanced InGaAs MSM-PDs and OE mixers

An understanding of device physics and accurate modeling of devices would help to develop better devices. With this motivation in mind finite volume modeling of MSM photodetectors and OE mixers was performed using CFD-ACE+ SEMI module. InGaAs MSM photodetectors with InAlAs Schottky Enhancement Layers (SELs) with very low dark current have already been demonstrated [11-13]. First use of InGaAs MSM photodetectors as OE mixers utilizing InAlAs as Schottky Enhancement Layer (SEL) has already been demonstrated [13]. In this work Finite Volume based simulations were carried out for transient and DC response of the MSM photodetector and the results are compared with experimental ones. A close agreement between the two was observed.

The simulations were performed for 60 µm^2 devices with 3 µm finger width and 3 µm spacing. For InAlAs, *Matthiesen's* rule was used to determine the mobility of the alloy from that of constituent semiconductors.

$$\frac{1}{\mu^{AB}} = \frac{x}{\mu^{A}} + \frac{1-x}{\mu^{B}} + \frac{x.(1-x)}{C_{\mu}}$$

where µ and x are mobility and mole fraction of corresponding species and C_{μ} is the bowing parameter.

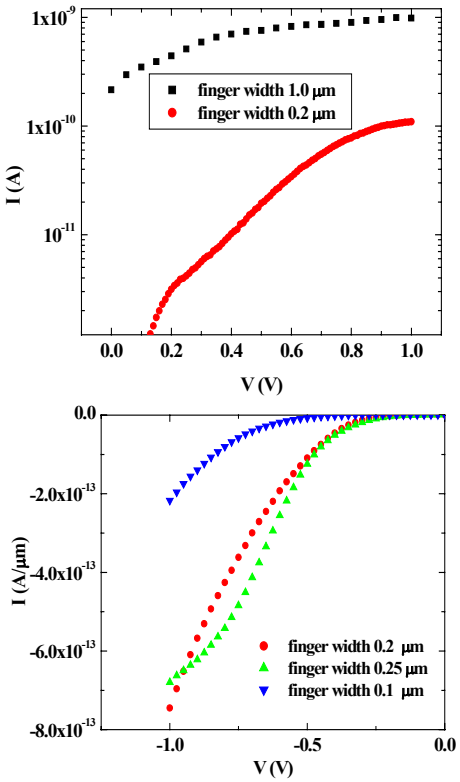

Fig. 3: Dark currents for MSM devices with (a) different finger width (b) different finger width but same periphery

For n–type material, a two–valley bowing parameter was used, whereas for p-type material a one–valley bowing

parameter was used. For InGaAs, a constant mobility model was used with electron mobility = 12000 cm^2/V-s and hole mobility = 300 cm^2/V-s. These values were obtained from the NSM webpage. Constant recombination life times were used for both the materials. For InAlAs, $\tau_{electron} = 1\times10^{-9}$ s, $\tau_{hole} = 2\times10^{-8}$ s, and for InGaAs, $\tau_{electron} = 1\times10^{-9}$ s, $\tau_{hole} = 1\times10^{-9}$ s were used. All other properties were used from the CFD-ACE-SOLVER data base.

Maxwell's equation can be reduced to the following equation

$$\frac{1}{\mu_0\mu_r}\nabla^2\vec{A}=\varepsilon_0\varepsilon_r\frac{\partial^2\vec{A}}{\partial t^2}+\varepsilon_0\varepsilon_r\frac{\partial\nabla\phi}{\partial t}+\sigma\frac{\partial\vec{A}}{\partial t}+\sigma\nabla\phi-\sigma(\vec{u}\times\vec{B})-\vec{J}_s$$

The equation is solved for vector magnetic potential, **A** and electrostatic potential ϕ. Convective current source is zero due to lack of any external Magnetic field in Z-direction. Light intensity I is given by the modulus of pointing vector, hence it can be seen that

$$I = \left|\vec{S}\right| \propto \left|\vec{A}\right|^2$$

where **S** is the Poynting vector given by

$$\vec{S} = \frac{1}{\mu}\vec{E}\times\vec{B}$$

where **E** is the electric field. To define the boundary conditions for the simulation, light intensity, *I* is used to calculate the magnitude of vector magnetic potential A at the surface, where it is varying in a sinusoidal manner. Inside the semiconductor, the power dissipation in each node can be found by taking the divergence of the Poynting vector. This term can be used to calculate the number of carriers generated in the semiconductor due to fundamental absorption process. Thus the semiconductor equations can be solved with the generation term G in the continuity equation calculated as above. The continuity equation is given by

$$q\frac{\partial n}{\partial t}-\nabla.\vec{J}_n = q(G-R)$$

$$q\frac{\partial p}{\partial t}+\nabla.\vec{J}_p = q(G-R)$$

where $\vec{J}_n$ and $\vec{J}_p$ are electron and hole current densities respectively, n and p the electron and hole densities respectively, q the electronic charge, G the generation rate of carriers and R the recombination rate of carriers.

(3) Pulsed Response

Spatial distribution of the carrier photo-generation rate was calculated and Figure 4 shows the electron and hole distributions just after the end of the light pulse and at two other time intervals from the removal of the light pulse. It can be seen that electron and hole distributions follow the power dissipation profile very closely. After the light pulse was switched off, the carriers were swept away by the bias and they were also terminated due to recombination.

Original photo-detector simulation had the light pulse on for sufficient period of time (10 ps) and then switched off. This methodology could not be used for the transient simulation of the InGaAs MSM detector, due to the short time period of the pulse (100 fs) which was incident on the detector. Instead, the transient simulations were divided into 3 different time period zones, depending on how fast the detector was switching. During the 100 fs time when the light was on the detector, a time period of 10 fs was used, during next 10^{-10} s, a time period of 10^{-12} s was used, and finally during last 9×10^{-10} s, a time period of 10^{-11}s, was used.

The pulse response simulation in Figure 5 shows a rise – time of 14 ps, and FWHM of 44 ps. The measured data gives rise time of 20 ps, and FWHM of

140 ps. The simulated detector is faster in its response compared to the measured device.

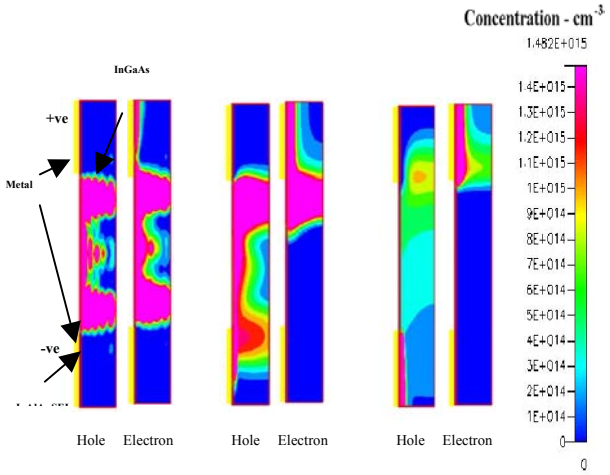

Fig. 4: Electron and hole distributions at the end of the (a) 100 fs long light pulse (b) after 5ps from removal of light pulse (c) after 215 ps from removal of light pulse.

(4) DC Response

To obtain the DC response of the detector, the simulation was setup for transient semiconductor simulation, with a very long total time for photo-generation. It was seen that the current converged to a constant value after some time. When higher light intensity was simulated, the time step had to be refined very much since the number of carriers was very large.

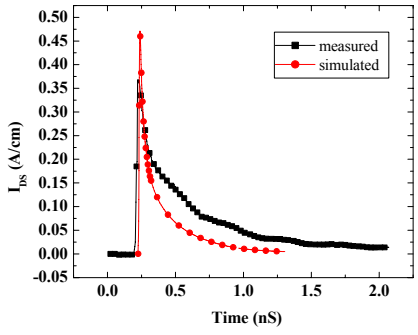

Fig. 5: Pulsed response of MSM photo detector (a) absolute value, (b) normalized

Figure 6 shows the DC response of the MSM–PD under illumination by 1.50 μm wavelength laser. A good match between the simulated and measured I-V curves was observed. The I-V curves exhibit a region where dI/dV transitions from a low value to a high value: this is referred to as a "knee". The "knee voltage" is defined as the bias at which the photocurrent equals 5% of the photocurrent at the second region where dI/dV is low.

As can be seen in Figure 7, the simulation predicts a decrease in knee voltage with decrease in SEL thickness. This is what is expected, in fact, it is expected that the tunneling current will increase so much that the knee would vanish altogether. The presence of 'knee' is also considered responsible for poor mixing efficiency of 500 Å SEL InGaAs-based OE mixers.

Figure 7 shows 2-Dimensional simulation of the MSM-PD response as a function of light intensity. The response for higher intensity light is slower compared to lower intensity light. The decrease in mobility caused by increased carrier generation is responsible for this "sluggish" behavior. Figure 7 shows simulated knee voltage as a function of light power and also as a function of Schottky Enhancement Layer thickness. Knee voltage increases both with increasing light intensity and with increasing Schottky Enhancement Layer thickness.

(5) Improving Performance of the OE Mixer

Schottky-enhanced InGaAs-based MSM-PDs do not operate well as OEMs. In particular, it was shown that the frequency bandwidth of such a mixer is much less than that of a corresponding photodetector. In addition, the mixing responsivity of the OEM was found to depend on the RF and LO signals and decreased non-linearly with decrease in optical power. The behavior of the InGaAs-based MSM-PD OEM was attributed to the large band-gap discontinuity associated with the SEL. One possible way to improve the mixing responsivity is

to reduce the ideality factor and enhance tunneling in the MSM-PD OEM. This may be achieved, for example, by reducing the ratio between the InAlAs SEL and the InGaAs active layer (or graded layer, if utilized).

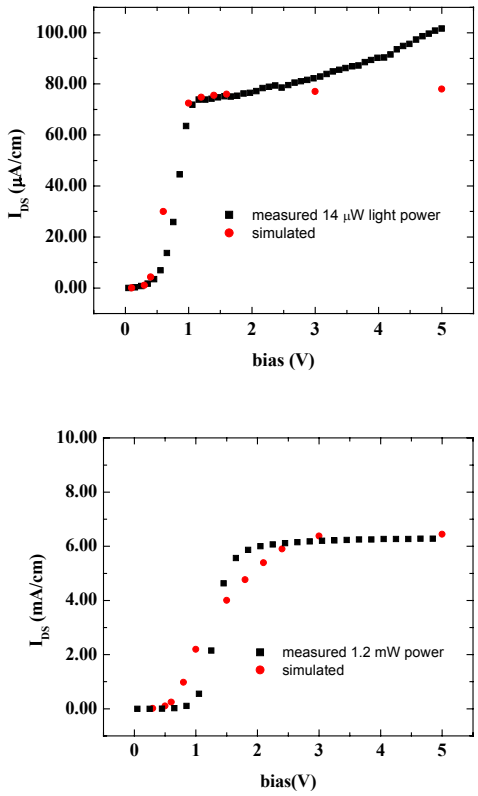

Fig. 6: (a) DC responsivity of 60 μm×60 μm MSM photodetector with 3 μm finger width and 3 μm finger spacing for two different light intensities. (b) DC responsivity of 60 μm×60 μm MSM photodetector with 3 μm finger width and 3 μm finger spacing for different SEL thicknesses and 14 μ W light intensity.

Based on the simulation for the effect of SEL thickness on the knee voltage, devices with two different SEL thicknesses were fabricated. We compare the mixing characteristics of a conventional InAlAs Schottky-enhanced InGaAs MSM-PD (SEL thickness of 500 Å) to that of an InAlAs Schottky-enhanced InGaAs MSM-PD OEM with a thin SEL (100 Å). For the thin SEL, the mixing characteristics are found to improve: The bandwidth of the optoelectronic mixer is similar to that of a corresponding photodetector and the mixing response de-creases only slightly with decrease in optical power. These results represent the first report of efficient optoelectronic mixing in InGaAs-based MSM-PDs.

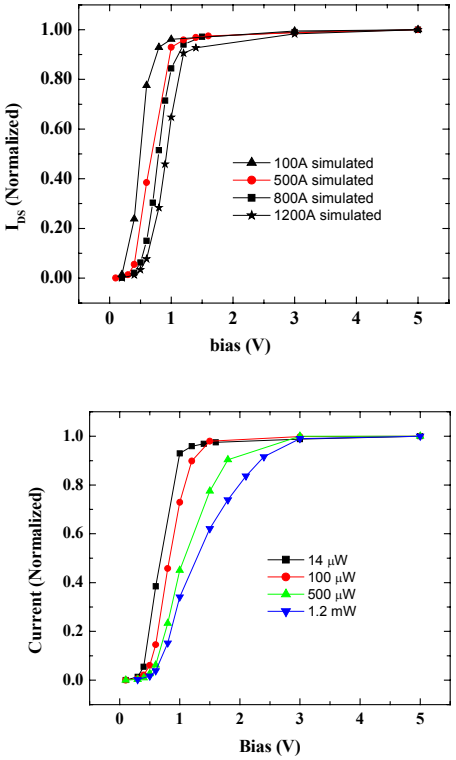

Fig. 7: (a) Simulated response of InAlAs/InGaAs OE mixer for different light intensities. (b) Simulated knee voltage as a function of light power and also as a function of Schottky Enhancement Layer thickness

In Figure 8, the responsivity of a 500-Å InAlAs Schottky-enhanced InGaAs MSM-PD (DC bias, RF light modulation) is compared to the responsivity of the same MSM-PD when operating as an OEM (LO bias, RF light modulation). Notice that the RF bandwidth of the MSM-PD OEM is much less than the RF bandwidth of the MSM-PD.

To compare the behavior of MSM-PD OEMs with differing geometries and device structures, it is convenient to define a "mixing efficiency" (M_{eff}). We define M_{eff} as the ratio of the responsivity of the MSM-PD OEM at the IF (mixed signal) frequency to its ideal DC responsivity. Figure 8 compares M_{eff}, as a function of RF frequency, for 100-Å and 500-Å thick InAlAs

Schottky-enhanced MSM-PD OEMs. There is a marked improvement in M_{eff} for the 100-Å MSM-PD OEM. In addition, the bandwidth of the 100-Å MSM-PD OEM is >1.0 GHz while the bandwidth of the 500-Å MSM-PD OEM is <200 MHz.

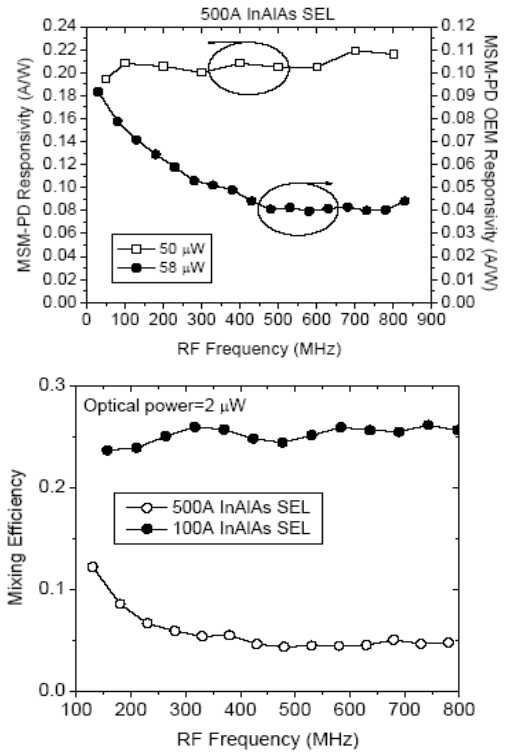

Fig. 8: (a) Responsivity of a MSM-PD (DC bias, RF light modulation) compared with the responsivity of a MSM-PD OEM (LO bias, RF modulation), as a function of RF frequency, for an InAlAs Schottky-enhanced device with a 500-Å thick SEL. (b) Mixing efficiency, as a function of RF frequency, of an InAlAs Schottky-enhanced MSM-PD OEM with a 100-Å SEL (solid circles) compared with the mixing efficiency of an InAlAs Schottky-enhanced MSM-PD OEM with a 500-Å SEL (open circles).

Acknowledgements

The work in UF is supported by an ARO grant (DAAD 19-01-1-0756).

References

[1] R. Johnson, *IEEE J. of Quantum Elec*., vol. 3, no. 6, pp. 232, 1967.

[2] T. Takahashi, K. Goto, Y. Higuchi, *IEEE J. Of Quantum Elec*., vol. 5, no. 6, pp. 328-329, 1969.

[3] A. Hughes, J. O'Shaughnessy, E. Pike, *IEEE J. of Quantum Elec.,* vol. 8, no. 12, pp. 909-910, 1972.

[4] J. T. Sackos, R. O. Nellums, S. M. Lebien, C. F. Diegert, J. W. Grantham, T. C. Monson, *Proc. SPIE*, vol. 3380, pp. 327-342.

[5] A. Gelbart, B. Redman, R. S. Light, C. A. Schwartzlow, A. J. Griffis, *Proc. SPIE*, vol. 4723, pp. 9-18.

[6] J. L. Eaves and E. K. Reedy, "Principles of Modern Radar," Van Nostrand Reinhold Company, New York, 1978.

[7] W. Ruff, J. Bruno, S. Kennerly, K. Ritter, P. Shen, B. Stann, M. Stead, G. Sztankay, M. Tobin, *Proc. SPIE*, vol. 4035, pp. 152-162, 2000.

[8] B. L. Stann, W. C. Ruff, Z. G. Sztankay, *Optical Engineering,* vol. 35, no. 11, pp 3270-3278, 1996.

[9] B. L. Stann, *et al*., "*Proc. of Advanced Sensors Consortium*, pp. 25-32, 2000.

[10] P. H. Shen, *et al*., *Proc. SPIE,* vol. 4028, pp. 426-435, 2000.

[11] Julian B., Soole D. and Hermann Schumacher, IEEE Journal of Quantum Electronics, 27(3), 7373 (1991).

[12] W. A. Wohlmuth, M. Arafa, A. Mahajan, P. Fay, and I. Adesida, Applied Physics Letters, 69 (23), 3580 (1996).

[13] E. Dröge, E. H. Böttcher, St. Kollakowski, A. Strittmater, D. Bibmberg, O. Reimann, R. Steingrüber, Electronics Letters, 34 (23), 2241 (1998).

[14] K. Aliberti, M. Wraback, M. Stead, P. Newman, and H. Shen, Applied Physics Letters, 80 (16), 2846 (2002).

[15] W. A. Wohlmuth, P. Fay, C. Caneau and I. Adesida, Electronics Letters, 32 (3), 249 (1996).

[16] H. Shen, K. Aliberti, B. Stann, P. Newman, R. Mehandru, and F. Ren, Applied Physics Letters, 82 (22), 3814 (2003).